Original Article

Damage detection in a composite wind turbine blade using 3D scanning laser vibrometry

Ryan Marks[1], Clare Gillam[1], Alastair Clarke[1], Joe Armstrong[2] and Rhys Pullin[1]

Abstract

As worldwide wind energy generation capacity grows, there is an increasing demand to ensure structural integrity of the turbine blades to maintain efficient and safe energy generation. Currently traditional non-destructive testing methods and visual inspections are employed which require the turbine to be out-of-operation during the inspection periods, resulting in costly and lengthy downtime. This study experimentally investigates the potential for using Lamb waves to monitor the structural integrity of a composite wind turbine blade that has been subject to an impact representative of damage which occurs in service. 3D scanning laser vibrometry was used to measure Lamb waves excited at three different frequencies both prior to, and after, impact to identify settings for an optimal system. Signal processing techniques were applied to the datasets to successfully locate the damage and highlight regions on the structure where the Lamb wave was significantly influenced by the presence of the impact damage. Damage size resulting from the impact was found to correlate well with the laser vibrometry results. The study concluded that acousto-ultrasonic based structural health monitoring systems have great potential for monitoring the structural integrity of wind turbine blades.

Keywords

Damage detection, NDT, wind turbine blade, 3D laser vibrometry, acousto-ultrasonics, Lamb waves,

BVID, Structural Health Monitoring

[1] Cardiff School of Engineering, Cardiff University, Cardiff, UK
[2] Polytec Ltd. Hertfordshire, UK

Corresponding author:
Ryan Marks, Cardiff School of Engineering, Cardiff University, Cardiff, CF24 3AA, UK.
Email: marksra@cardiff.ac.uk

Introduction

As technology continues to advance and world population increases there is an ever increasing demand for energy. Due to limited reserves of fossil fuels and increasing pressure to reduce environmental impact, renewable methods of producing energy are forming an increasingly important part of the world's energy capacity.

A long established alternative to fossil fuel power generation is wind energy. Globally, 51,477 MW of new wind power capacity was added in 2014 with the UK contributing 1,736 MW (3.4%) of generation, bringing the total global wind generation capacity at year end to 369,553 MW[1].

To maintain optimum performance of the wind turbine fleet, the structural integrity of the turbine has to be ensured. Blade failures are the most common structural failure on a wind turbine[2, 3] with tip breaks being the most prevalent type of blade failure. Although the blades typically represent less than 20% of the overall capital cost of the turbine, they are the biggest source of maintenance costs[4]. Data from in-service operation of wind turbines has shown that the blades have the second highest failure rate of all of the components of the turbine[5].

Of the wind turbines currently in operation, 51% of blade damage is attributed to manufacturing defects whereas 49% of damage is as a result of in-service operation. Of all damage events, 16% of all damage is attributed to foreign object damage while the turbine blade is in-service (with lightning strikes (20%) and the tips deflecting causing them to hit the tower (13%) making up the rest of the 49%)[6]. In optimum wind conditions, large wind turbine blade tips can move through the air at relative speeds of up to 320 km/h (200 mph)[7] making impacts from even small objects significant. Damage to both the leading edge and blade surface (from rain, hail, ice, sand, salt, UV rays and insects)[8] is detrimental to aerodynamic efficiency and as a result power generation is compromised. Serious structural damage can also be caused by lightning and bird strikes. A detailed discussion of turbine blade damage is presented in a study conducted at Risø National Laboratory[9].

Small impacts can create barely visible impact damage (BVID) which, if allowed to grow under the aerodynamic loading, could necessitate significant repair works or result in catastrophic failure of the blade structure. BVID is a term used that depends on many factors such as colour of the structure, illumination and angle of viewing[10] although it has been suggested that BVID usually lies within the range of 0.25 - 0.5 mm[11]. Non-destructive testing (NDT) methods are currently conducted to detect BVID however blade removal is usually required. Maintaining the structural performance of the blades is therefore vital to the turbine's efficiency[12].

It is recommended that wind turbine blades undergo a full in-service visual inspection on a yearly basis to significantly reduce the risk of catastrophic failure[12]. Visual inspection and traditional NDT techniques are currently employed for installed blade maintenance, although due to turbine size (ranging from 26 - 128m),[5] height and blade location these are costly, lengthy processes that are subject to human error.

There are currently condition monitoring (CM) and supervisory control and data acquisition (SCADA) systems in place in which fault detection and diagnostic algorithms are implemented to provide an early warning system[13]. However, the data received only detects the fault based on the response of the turbine to damage and does not characterise or locate it. SCADA and CM systems monitor a large range of parameters, including direct wind measurements, vibration, temperature and the efficiency of the energy conversion process (e.g. power output, blade pitch angle, rotor speed). There is currently typically only a 60 minute window between detection and failure when using a SCADA system[8]. Structural health monitoring (SHM) studies suggest that defects could be detected long before they have an adverse effect on the performance of the system[14]. There are many SHM techniques which are currently being developed to continually monitor the structure of wind turbine blades for damage. Acoustic Emission (AE) is a powerful SHM technique a which is showing a great deal of potential. Many laboratory and field based

studies have been conducted using this technique.[15-18] This technique benefits from being a passive technique meaning that no external excitation is required and can be used for detecting and locating a range of damage mechanisms.[19] However, the drawback to technique is that other acoustic signals (such as mechanical noise from the gearbox) may be incorrectly interpreted as a damage signal.

Thermal imaging methods have become an important tool for SHM of wind turbines. This is typically split into two approaches; active and passive. The passive approach is beneficial as it can be conducted while the wind turbine is in operation from the ground by differences in temperature to that of ambient although the development of this techniques is still at an early stage[20]. The active approach requires thermal excitation to create the thermal contrast on the turbine blade highlighting regions of high stress and hence damage. Techniques such as thermoelastic stress method have shown great potential for the monitoring of wind turbine blades[21-23].

Modal-based techniques have been a common method of conducting SHM[24] on wind turbine blades[25, 26]. The structure is either excited from the ambient modal response during operation or from some external excitation such as a shaker. The modal response is measured by sensors on the structure or other vibration measurement technique such as laser vibrometry[27]. When damage is present, such as fatigue cracks which affect structural stiffness, the response changes. By comparing this response with the healthy state, the presence of damage can be identified and to some degree localised.

Fibre optic methods have become a popular method of monitoring blade structural performance. Fibre optics can be used to measure the light intensity along the length of the fibre. As the structure is loaded, the fibre deforms reducing the light intensity and hence the loading can be monitored for the onset of damage. Fibre Bragg gratings use a series of grates which reflect a narrow band of a broadband light source. As the structure deforms, the grating varies causing the wavelength of light reflected light to vary.

This has been used to some success in monitor crack growth[28] and impact damage[29] as well as showing potential to sense AE sources[30-32]. These technique can be applied to both new and in-service blades.

A summary of commonly used SHM techniques have been presented here although there are many other SHM methods such as eddy current monitoring, electrical resistance and vacuum pressure monitoring used in other applications[33]. Comprehensive reviews of studies for the SHM for wind turbines are presented by Yang et al.[34] and Ciang et al.[13]

By implementing a cost-effective SHM system the down time of the turbine will be reduced and overhaul logistics can be optimised and pre-planned; lowering the turbine's life cycle costs[13]. This is particularly significant for turbines installed in remote areas such as offshore.

A long-established technique for detecting damage in structures is by using acousto-ultrasonic-induced Lamb waves. The principle involves exciting a piezoelectric transducer mounted to the structure's surface which induces a Lamb wave that propagates through the structure and is then detected by another transducer mounted at a different location on the surface. If damage occurs within the transmission path between the two sensors, the signal propagation is altered resulting in a quantifiable difference in the signal received. This technique can be extended to networks of multiple sensors to improve detection capability.

Following a review of Lamb wave based studies using laser vibrometry to detect impact damage in composite components for SHM applications, this paper presents the results of an experimental study into the interaction of Lamb waves with impact damage on a composite wind turbine blade using 3D scanning laser vibrometry. Visualisation of both this out-of-plane and in-plane components of the Lamb wave interaction with impact on a real structure is presented. Results showing Lamb wave interaction

along with post-processing of the vibrometry data using RMS baseline subtraction techniques are presented and discussed. Novelty is found within this study with the consideration of both of the components (particularly the in-plane) and the visual and signal processing methods used to present the interaction with the impact damage. This advances understanding of the interaction of the different fundamental Lamb modes as well as highlighting areas suitable for the placement of sensors for an acousto-ultrasonic system. The results are further compared to surface profilometry and white light interferometry measurements of the impact site. The extent of the impact damage was considered to be 'barely visible'. The surface measurements are shown to correlate with the interaction of the Lamb waves shown in the laser vibrometry results, demonstrating the sensitivity of Lamb wave-based SHM systems to detect impact damage.

Lamb waves

Lamb waves are traction free plate waves first observed by Lamb[35]. Through the combination of shear and pressure components two main modes of a Lamb wave are formed; symmetrical (S) or extensional modes which can be represented by cosine functions, and asymmetric (A) or flexural modes which can be represented by sine functions. The full numerical solutions are presented by Rose[36].

Dispersion is a phenomenon where the velocity of a Lamb wave is a function of its excitation frequency. This is an important consideration for pulse-receive type SHM systems where detecting damage is dependent on the wavelength of the Lamb wave. The mathematical solutions to Lamb waves demonstrate there are two variables that determine the dispersion of a Lamb wave, the frequency and the plate thickness. This is known as the frequency-thickness product. By using this relationship it is possible to calculate higher order modes of Lamb waves[37]. The fundamental modes of S_0 and A_0 are only typically

excited in an SHM system. If higher order modes are excited, their amplitude tends to be considerably less than that of the principle modes meaning that their use in SHM systems is limited[38].

There have been many studies conducted using acousto-ultrasonic Lamb waves to detect the presence of damage on a structure. Pullin *et al.* successfully used acousto-ultrasonic Lamb waves to detect the presence of impact damage on a scale carbon fibre wing structure[39]. Measurements of Lamb waves were taken pre and post impact using macro-fibre composite (MFC) transducers. By using the pre-impact measurements as a baseline, a quantitative comparison of the received waveforms was made using a cross-correlation technique. The analysis showed a significant change in the wave form by a reduction in cross-correlation coefficient as well as demonstrating the potential for energy harvesting using acousto-ultrasonic Lamb waves. However, the interaction of the waves with the damage could not be observed visually unlike the results presented in this study.

Laser vibrometry

3D scanning laser vibrometry is a non-contact vibration measurement technique. The technique uses three laser heads to measure the Doppler-shift between the backscattered light and a reference signal. This is proportional to the vibrational velocity. Through trigonometric techniques both in-plane and out-of-plane velocities of vibration are measured.

Scanning mirrors allow the lasers to be steered making it is possible to measure vibration at multiple locations on a structure in a relatively short period of time. This enables a full-field 3D representation of a wave to be created.

As laser vibrometry is a non-contact measurement technique, the presence of additional sensor mass on the structure which may contribute to mass dampening is eliminated. The technique is broadband and has a transfer function of unity allowing an accurate measurement of Lamb waves to be made[40, 41].

Laser vibrometry damage detection studies

Laser vibrometers were first developed as a measurement tool in the 1980s but had limited sensitivity and low signal-to-noise ratio (SNR) limiting their application. Substantial advances in computation during the 1990s, the instrumentation became mature enough for widespread use[42]. Vibrometry technology advanced further towards the end of the last century reaching maturity level making it possible to measure ultrasonic elastic waves.[43-46]. The technique was soon after developed further and applied to detecting defects in composite materials using Lamb waves[47-49].

Laser vibrometry has been used to inspect turbine blades for damage in many studies[50-52]. The focus of these studies however has been to investigate modal responses of healthy and damaged blades. The results from these studies do not locate or characterise the damage using ultrasonic techniques, which is the explicit aim of the work reported in this paper.

There is limited published works using laser vibrometry and ultrasonic techniques to assess the structural integrity of wind turbine blades. A study by Lee *et al.*[6] investigated the viability of using a pylon mounted laser vibrometer with integrated transducers used to initiate a Lamb wave as a non-contact method which can inspect the full length of the turbine blade. The focus of the study was the development of a cost-effective, portable laser vibrometer for in-service monitoring of wind turbine fleets. Image processing techniques were used to quantitatively compare baseline images with images that showed the presence of damage. The result of the analysis gave a visual representation of the damage and its location. The

main focus of this study was the interaction of Lamb waves with damage for the development of an SHM system comprised of a network of sensors but rather the development of a laser vibrometer for in-service use.

Aside from the applied study of wind turbines, studies have been conducted using laser vibrometry to investigate Lamb wave interaction with impact damage in composites. A study by Grigg *et al.*[53] investigated Lamb wave interaction with impact damage in a flat carbon fibre panel using 3D scanning laser vibrometry. The results showed little interaction of the S_0 mode with the impact damage but a significant disruption to the propagation of the A_0 mode. It was found that the presence of the impact damage had a greater effect on Lamb waves of higher frequencies.

Schubert *et al.*[54] investigated Lamb wave interaction with impact damage in carbon fibre reinforced plastics using 3D scanning laser vibrometry. It was found that the A_0 mode showed the strongest interaction with the damage. Phase-based techniques were used to evaluate the time signal difference before and after damage and a ratio of the energy of the out-of-plane component was obtained. The study concluded that phase based signal processing was more sensitive to impact damage than amplitude based methods

A study by Sohn *et al.*[55] investigated Lamb wave interaction with impact induced delaminations in composite plates using a 1D scanning laser vibrometer to measure the out-of-plane component of Lamb waves. The measurements were post-processed using an outlier analysis to quantify the size and shape of the damage. Frequency-wavenumber domain and Laplacian image filters were also applied to measurements to enhance the visualisation of the defects. The technique was also applied to delaminations of composite stiffeners highlighting the potential for image based techniques for SHM applications.

Staszewski *et al.*[56] used 3D laser vibrometry to measure Lamb waves generated by a piezo-ceramic transducer bonded to the surface of an aluminium plate. A fatigue crack was grown in the aluminium specimen from a spark eroded notch. The interaction of Lamb waves excited at 75, 190 and 325 kHz with the fatigue crack was investigated. The capability of the 3D vibrometer was exploited allowing an in-depth study of the interaction of both S_0 and A_0 modes with the damage to be conducted.

Experimental study

A commercial 1.8m composite wind turbine blade constructed from a short glass fibre chopped strand mat with a black epoxy matrix was used for this study, as shown in Figure 1. The placement of the fibres was random and hence the direction of the fibre placement was inhomogeneous (N.B. this is not in reference to the material properties being inhomogeneous). The structure of the blade was hollow, made from two 3mm thick matched halves bonded together.

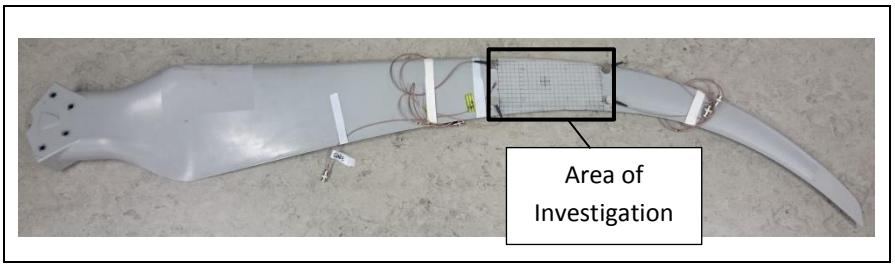

Figure 1. Composite wind turbine blade used throughout the experiments, demonstrating the location of the area of investigation.

An area of investigation of dimensions 50mm x 120mm was located on the low pressure face 1.17m from the root of the blade as shown in Figure 2.

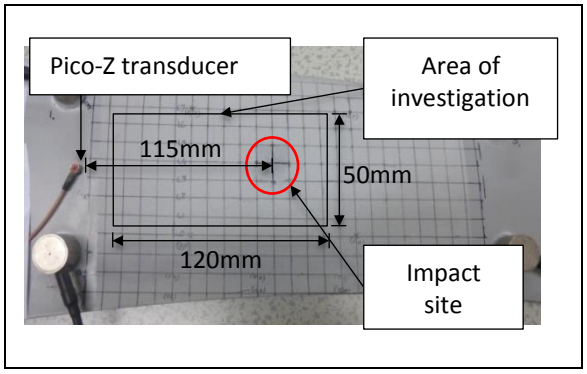

Figure 2. Dimensions of the area of investigation and location of the impact

The transducer selected for this study was a commercially available PANCOM Pico-Z (200kHz – 500kHz) which was acoustically coupled to the blade using Loctite® Ethyl-2-Cyanoacrylate adhesive. The small face size of this sensor makes it more representative of a point source than a larger sensor. The frequency response within the operating range is also relatively flat. The transducer was located at a distance of 115mm from the impact site. This was sufficient distance to ensure that that the Lamb waves had fully formed before interacting with the impact damage.

3D scanning laser vibrometry setup

Three transducer excitation frequencies of 100kHz, 200kHz and 300kHz were selected to investigate the sensitivity of different wavelengths to the presence of impact damage. Although 100kHz lies outside of the published operating resonance of the transducer it has shown to produce useful results in previous studies[53, 57, 58]. Due to the maximum sampling frequency of the vibrometer being 2.56MHz, frequencies above 300kHz were not considered due to insufficient temporal resolution

A 150V, 5-cycle sine burst was generated by a Mistras Group Limited (MGL) WaveGen function generator software which was connected to MGL µdisp/NB-8 hardware. A 10 V peak-to-peak reference signal was

also generated to trigger the acquisition of the vibrometer. A repetitive trigger rate of 20 Hz was used as it gave sufficient time for the Lamb wave to attenuate between bursts.

A Polytec PSV-500-3D-M Scanning Vibrometer was used for this study. The area of investigation comprised of 2514 measurement points which gave sufficient spatial resolution for wave reconstruction. To improve the signal-to-noise ratio the area of investigation was coated with retro-reflective glass micro-beads. 200 measurements at each point were recorded, and the average calculated to further improve the signal to noise ratio.

4096 samples were taken giving an overall sample time of 1.6 ms and a resolution of 390.625 ns.

Two sets of measurements were taken; prior to impact, which served as a baseline, and after impact.

A purpose built steel stanchion was used to support the turbine blade while the laser vibrometry measurements were taken. This allowed the blade to be removed for impacting and replaced in the same position relative to the laser heads.

Impact Damage

The blade was secured at the base to a steel stanchion and supported on both sides of the area of investigation. The blade was impacted using a 20mm radius impactor with impact energy of 10 Joules in an INSTRON dynatup 9250HV impact test machine. The impact caused BVID on the surface as shown in Figure 3. The impact was representative of a hail stone impact.

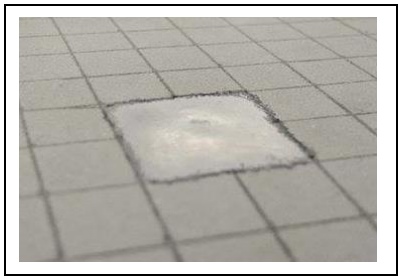

Figure 3. BVID on the turbine blade after being impacted. The retro-reflective beads have been removed around the impact site for clarity.

Laser vibrometry results and discussion

For each set of results, a 0μs datum point was taken immediately as the S_0 mode reached the measurement field. A selection of images are then shown in Figures 4 to 12 which illustrate the propagation of the Lamb waves through the area of investigation. For consistency, the time windows for each excitation frequency have been kept the same. As wave velocity increases with frequency due to dispersion, fewer images are presented for the higher frequency excitations. For each set of post-impact measurements, the white dashed line denotes the impact site.

100kHz results

The results of the resultant magnitudes (the magnitude calculated from the three components measured by the vibrometer) from the pre and post impact scans are shown in Figure 4 and Figure 5 respectively.

Studying the pre-impact results, it is apparent that the S_0 mode propagated away from the source and appears either not to reflect off the edges of the turbine blade or has dissipated by that point, or by the time any reflections have reached the area of investigation.

The A_0 mode however appears to be significantly disrupted as it propagated through the area of investigation. There are two explanations for this. The first is the interaction of edge reflections with the propagating wave. However it is also likely that the scattering of the A_0 mode observed is the result of the

fibre distribution in the material. As the fibres are randomly distributed, it results in a inhomogeneous microstructure [59]. This can cause scattering of the Lamb waves which results in a high level of noise in the propagating wave[60]. This is observed from 90µs onwards.

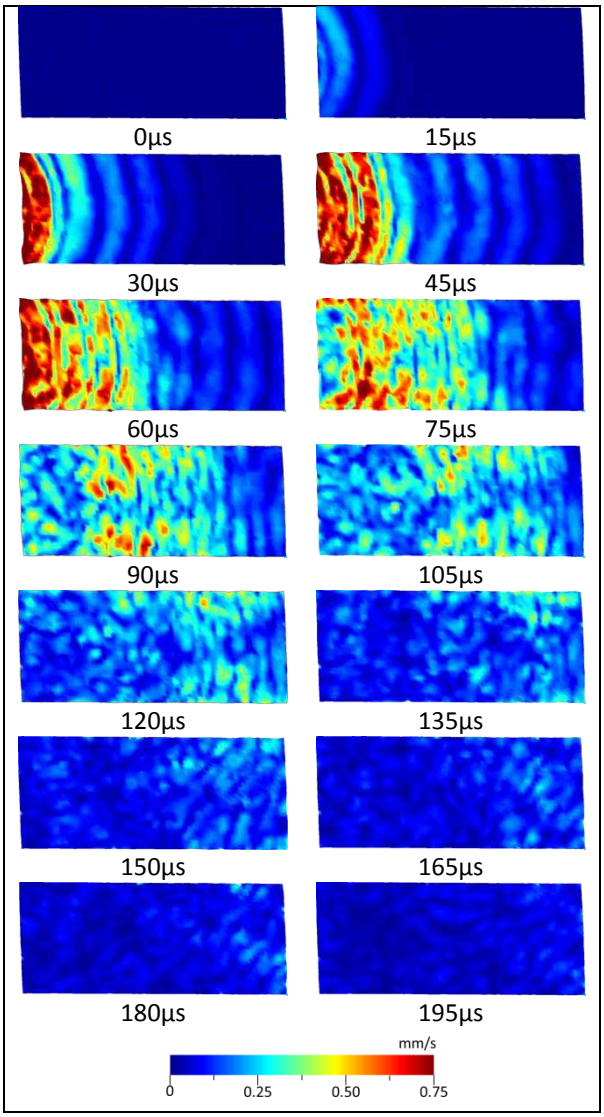

Figure 4. Resultant magnitude results of the 100kHz excitation vibrometry scan of the blade pre-impact

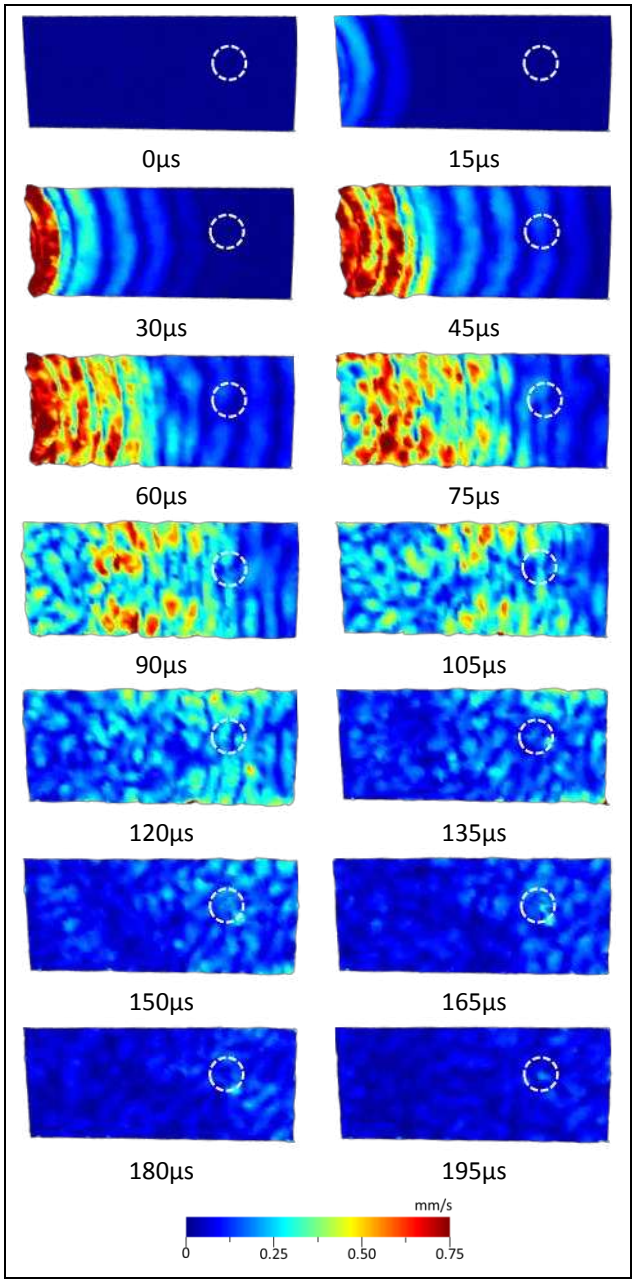

Figure 5. Resultant magnitude results of the 100kHz excitation vibrometry scan of the blade post-impact

Comparing the two sets of results, the S_0 mode appears to be mostly unaffected by the presence of the impact damage. This concurs with the findings of Grigg *et al.*[53]. The A_0 Lamb mode does appear however

to be affected by the presence of the impact damage. This can be seen in the results at 90µs - 120µs although it is not clear when the resultant magnitude is plotted.

As the A_0 Lamb mode is mostly out-of-plane, this component was isolated and plotted separately for clarity as shown in Figure 6. It is evident that the out-of-plane component of the Lamb wave interacts with the damage causing a disruption in the wave front. This suggests that the unintelligibility of the interaction of the A_0 mode with the damage in the resultant magnitude plots in Figure 4 and Figure 5 is mostly caused by noise from the in-plane components.

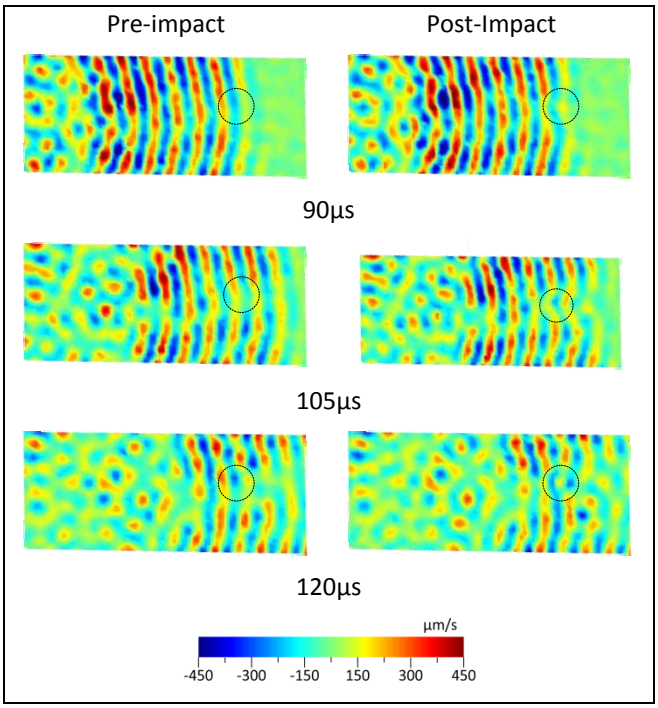

Figure 6. 100kHz excitation out-of-plane component highlighting the Lamb wave interaction with the impact damage

200kHz results

The results of the resultant magnitudes from the pre and post impact scans are shown in Figure 7 and Figure 8 respectively.

Comparing these results to those from the 100kHz excitation there is an increase in amplitude of the measured Lamb wave. This can be attributed to this 200kHz being inside of the transducer's operating resonance.

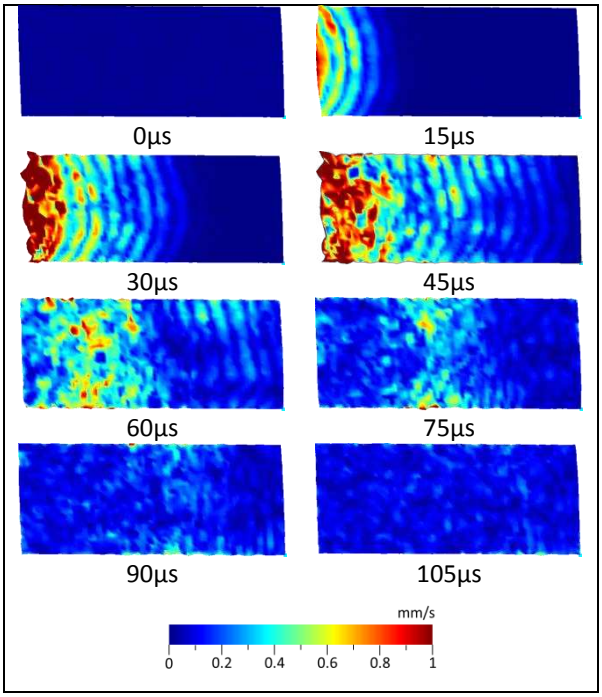

Figure 7. Resultant magnitude results of the 200kHz excitation vibrometry scan of the blade pre-impact

As with the results from the 100kHz excitation, the S_0 mode appears to be unaffected by the presence of the impact damage in the resultant magnitudes results. Comparing the S_0 propagation in both the pre and post impact results at 45µs it is not possible to distinguish the presence of damage by visual observation

alone especially as there appears to be no disruption in the wave front to the right of the impact damage as observed with the A_0 mode in Figure 6.

The effects of attenuation and dispersion of higher frequency waves, coupled with high levels of noise, resulted in a highly disrupted, low amplitude A_0 wave front by the time the mode reaches the impact site as shown at 90µs. As with the 100kHz results, this makes it difficult to determine whether the Lamb wave interacted with the damage through means of visual observation alone.

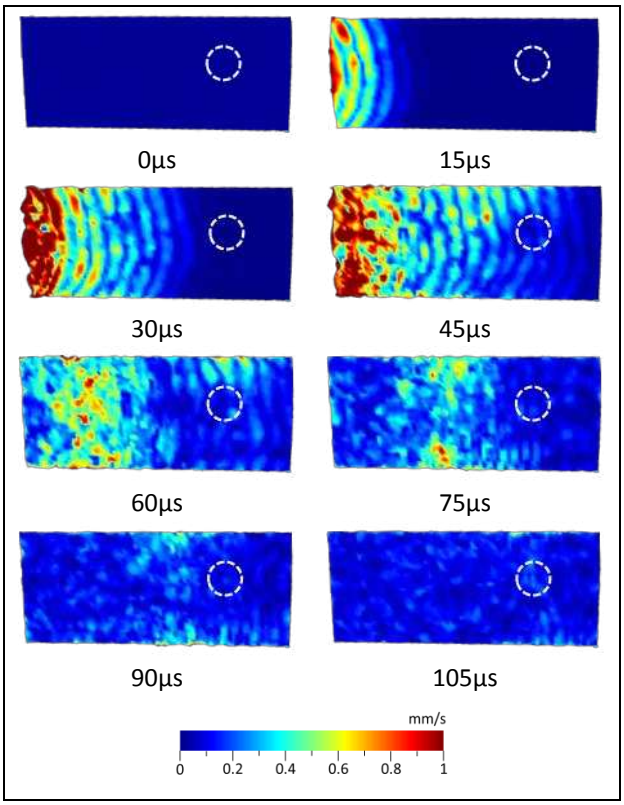

Figure 8. Resultant magnitude results of the 200kHz excitation vibrometry scan of the blade post-impact

To verify the Lamb wave interaction, again the out-of-plane component was isolated and plotted separately as shown in Figure 9.

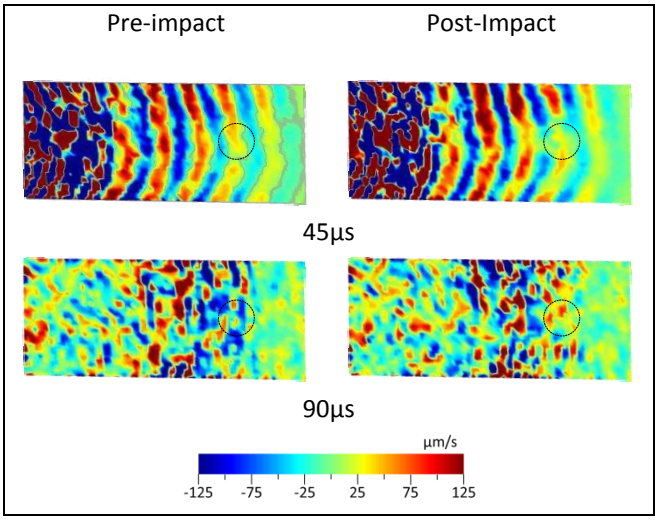

Figure 9. 200kHz excitation out-of-plane component highlighting the Lamb wave interaction with the impact damage

The results at 45µs show that there is possibly some interaction with the S_0 mode. This may be indicated in the post-impact results where there is a significantly lower amplitude than in the pre-impact results due to the presence of the impact damage. This can be justified by the shorter wavelength of the 200kHz excitation S_0 mode compared to that of the 100kHz excitation. However, there appears to be no disruption in the wave front to the right of the impact site which also suggest that there is limited interaction with the impact damage. It is therefore not conclusively possible to determine the presence of the impact damage using the S_0 mode from the 200kHz excitation by visual observation alone.

It is difficult to determine from these results whether the A_0 mode is influenced by the presence of the damage as demonstrated at 90µs. It is apparent there is a difference in the results and it could be argued that the reduction in amplitude in the post-impact results was due to the presence of the damage. However, due to the high levels of disturbance in the wave front this is also by no means conclusive.

300kHz results

The results of the resultant magnitudes for the pre and post impact 300kHz excitation are shown Figure 10 and Figure 11 respectively.

The increased wave velocity due to dispersion is apparent when compared to the results of the 100kHz excitation. As with the two other excitation frequencies, the S_0 mode in the resultant magnitude results appears to be mostly unaffected by the impact damage. However, by the time the S_0 mode interacts with the impact damage, the amplitude has significantly reduced.

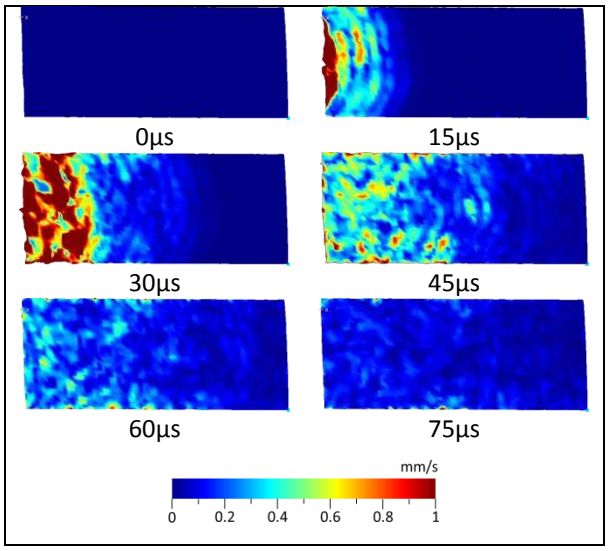

Figure 10. Resultant magnitude results of the 300kHz excitation vibrometry scan of the blade pre-impact

The increased attenuation of the higher frequency excitation is apparent in this results set. The A_0 mode is measured in the area of investigation with a peak amplitude of 1mm/s. At 45µs the amplitude of the wave has significantly decreased. This decrease in amplitude with the added effects of edge reflections and scattering due to the microstructure makes it near impossible to determine Lamb wave interaction from just studying the resultant magnitude time-domain results alone. In turn, adjusting the colour scale to study the low amplitude Lamb wave activity does not help to clarify the results.

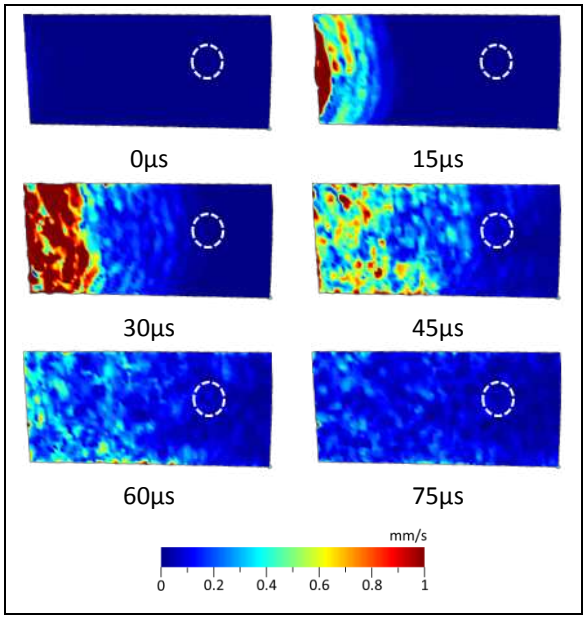

Figure 11. Resultant magnitude results of the 300kHz excitation vibrometry scan of the blade pre-impact

As with the results from the previous two excitation frequencies, the out-of-plane mode was isolated and presented in Figure 12.

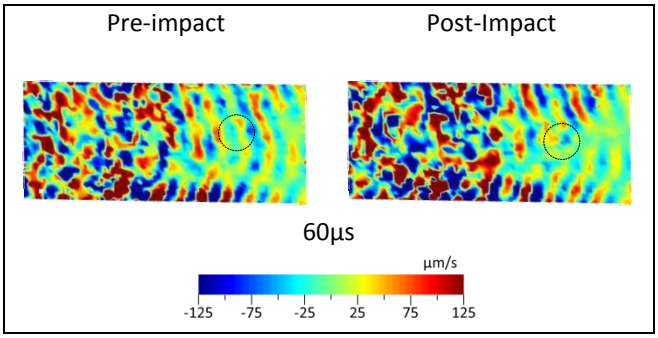

Figure 12. 300kHz excitation out-of-plane component highlighting the Lamb wave interaction with the impact damage

As with the 200kHz excitation, the S_0 mode interacts with the damage. This is shown in the post-impact results by a fringe of low amplitude to the right of the impact damage. However, as also with the 200kHz excitation, due to the high levels of disturbance in the wave it is not possible to determine A_0 mode interaction with the damage.

The clarity of the wave propagation may be improved upon by increasing the number of scan points, hence increasing the spatial resolution for the higher frequency excitations. However, for comparability between excitation frequencies and constraints on acquisition time this was not changed during this study.

Root-mean squared baseline subtraction

From the time domain results presented, it is apparent that the A_0 Lamb mode does interact with the damage although it is difficult to identify the presence of damage on the structure without carefully examining the results. It therefore would be advantageous to identify the presence of the BVID and quantify it using comparative post processing methods. A computationally inexpensive post-processing technique is baseline subtraction. Subtracting the waveforms of the out-of-plane component of the post-impact dataset from the waveforms of out-of-plane component from the pre-impact dataset identifies the region on the scan area where there is a significant change. By calculating the root-mean squared (RMS) velocity values for the resulting subtracted waveforms of each measurement point over the whole measurement period, the region of significant change in waveform, and hence the location of the damage can be identified. The RMS baseline subtraction analysis for the out-of-plane component of the Lamb wave is presented in Figure 13. Only the out-of-plane component has been considered as it was shown to significantly interact with the damage. The impact site is denoted by the dashed line.

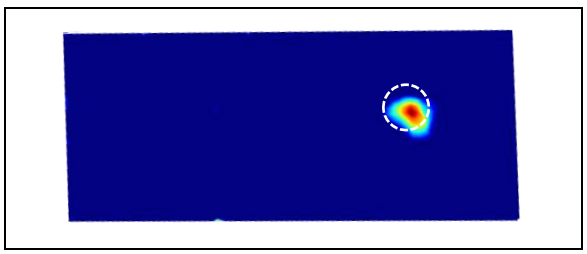

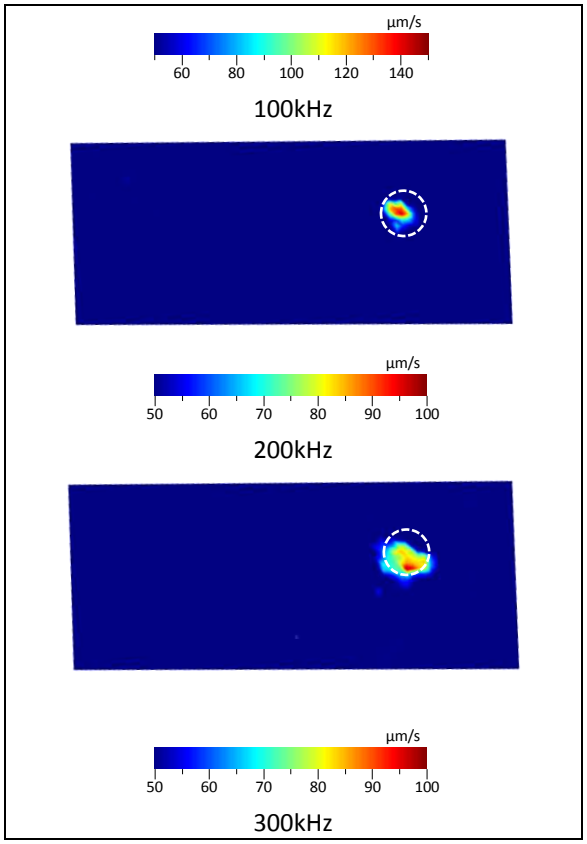

Figure 13. RMS baseline subtraction analysis of the out-of-plane component of the Lamb modes

For each excitation frequency the impact site has been clearly identified by this technique. The peak RMS values for the 100kHz excitation are greater than those for the 200kHz and 300kHz excitations. This is because of the lower attenuation of the lower frequency. The RMS values the plate area outside of the impact site are not zero. This is because of small differences in experimental setup between the pre and post impact vibrometry scans. This has resulted in a small phase difference which when subtracted results in low amplitude signals being produced. In addition to this, low amplitude reflections result due to Lamb wave interaction with the damage and hence cause an additional change in signal.

The size of the area influenced by the defect appears to vary depending on excitation frequency. Using the Polytec PSV software, it was possible to measure the size of the area of peak RMS. Taking

measurements across the peak for each excitation frequency found the average length of the area affected by the presence of the damage to be 12.6mm, 7.8mm and 14.9mm, for the 100kHz, 200kHz and 300kHz results respectively. Surprisingly the average length of the area affected by the presence of the damage increases from the 200kHz excitation results to the 300kHz excitation results as the reduction in wavelength should be more sensitive to the impact damage.

Out-of-plane cross-correlation

Calculating the cross-correlation coefficient of two waveforms has previously been used in acousto-ultrasonic studies as method of quantitatively comparing two waveforms[39]. A value for the cross-correlation coefficient of unity indicates no change in the waveforms. By comparing the measured signals pre and post-impact an indication may be obtained of where the wave has interacted with the damage. Results from the cross-correlation analysis for the out-of-plane component of the Lamb wave are presented in Figure 14. The impact site is denoted by the dashed line.

It is evident that the Lamb wave interaction with the impact damage significantly alters the waveform when compared to the pre-impact waveforms.

The results from the 100kHz excitation show that there is little difference in waveform in-front (left hand side of Figure 14) of the impact damage. There is a significant, localised reduction in correlation downstream (right) of the impact damage. There is an increased area of lower correlation behind the impact damage in the results from the 200kHz excitation. In addition to this, there is also a minor reduction in correlation in front of the impact damage. The 300kHz results show an increased area of lower correlation behind the impact damage when compared to the 200kHz results as well as reduced correlation in front.

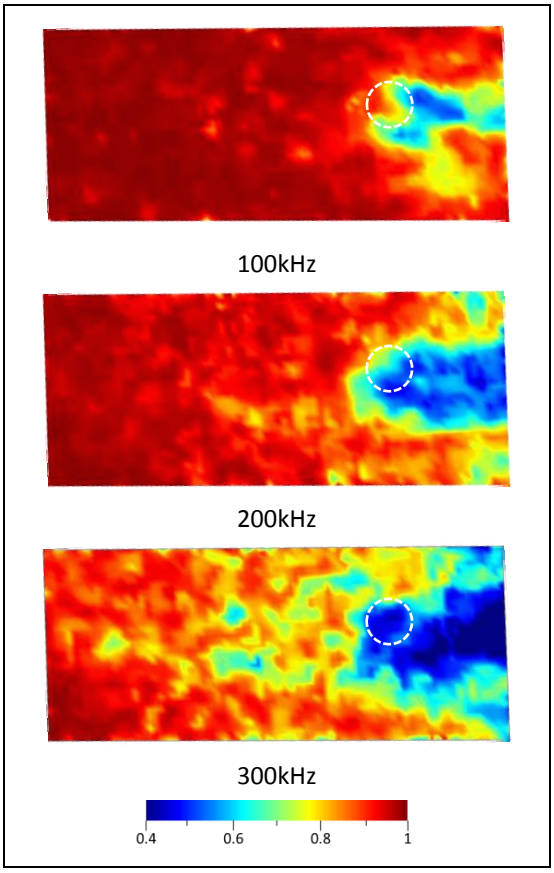

Figure 14. Out-of-plane cross-correlation coefficient results

The increased area of lower correlation demonstrates that higher frequency Lamb waves are more sensitive to interaction with damage due to their smaller wavelength. At the higher frequencies there is also a reduction in correlation in front of the impact damage. This is most likely due to reflections from the damage.

Previous studies that have used the cross-correlation technique have shown less difference in signals which was quantified by a smaller reduction in cross-correlation coefficient. It is worth noting however that previous studies used sensors physically coupled to the structure that have a mass-dampening effect

as well as a transfer function. In addition to this, cross-correlation coefficients have not been previously calculated at the impact site.

In-plane cross-correlation

Considering the in-plane components of the wave it is possible to conduct a cross-correlation analysis to investigate how the in-plane components are affected by the presence of the impact damage. This is conducted by calculating the respective cross-correlation coefficients for both of the in-plane components. The resultant magnitude of the two cross-correlation coefficients is then calculated. The theoretical maximum for the cross-correlation is therefore √2. In order to make the results comparable to the out-of-plane results, the cross-correlations coefficients are divided through by √2. The results of this analysis are presented in Figure 15. The dashed line denotes the impact site.

It is apparent that the propagation of the in-plane component of the Lamb wave is affected by the presence of the impact damage. The 100kHz results clearly indicate a difference in the two Lamb wave signals at the of the impact damage. Comparing this with the out-of-plane results it is evident that there is less reduction in cross-correlation coefficient in this region.

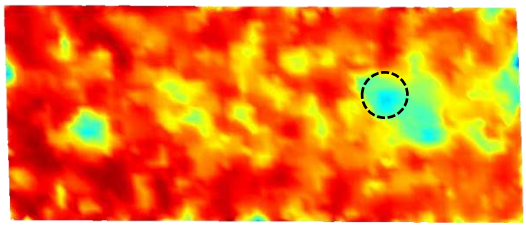

100kHz

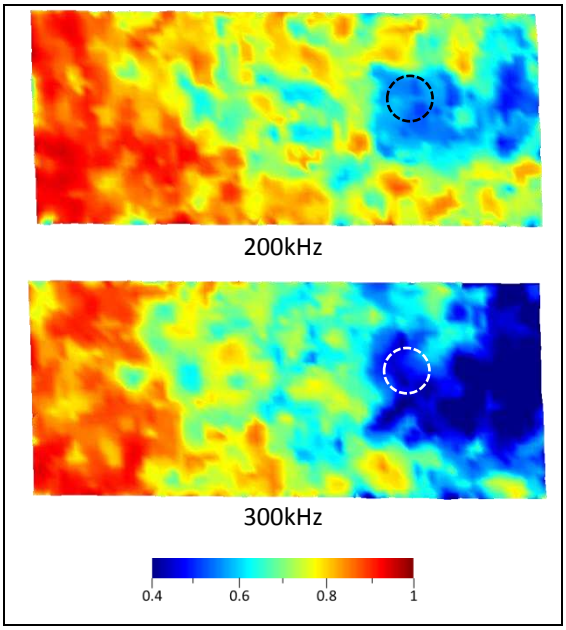

Figure 15. In-plane cross-correlation coefficient results

Unlike the out-of-plane results, there is a significant reduction in cross-correlation coefficient over a much larger region of the area of investigation. This can be justified by the scattering of the in plane modes due to the microstructure. It was demonstrated by comparing the resultant magnitude plots with the out-of-plane plots for the 100kHz excitation that a significant level of noise could be attributed to the in-plane components. This is due to the random placement of the chopped fibres. In fibre composite materials the in-plane Lamb wave components are influenced by the fibre direction[53] therefore inhomogeneity of the fibre directions will have a more significant influence the noise on the in-plane components than the out-of-plane.

The results from the 200kHz excitation identify a region of reduced cross-correlation coefficient surrounding the impact site. The region is larger than that of the 100kHz excitation and is similar to that observed in the out-of-plane results. This can be attributed to the shorter wavelength of the higher frequency excitation. Like the 100kHz excitation, there is a region of reduced cross-correlation coefficient

upstream of the impact site. This suggests that the in-plane component of the Lamb wave is partially reflected by the presence of the impact damage which is not possible to determine by studying the time-domain plots alone.

The results from the 300kHz excitation show a large region of the area of investigation where there is a significant reduction in cross-correlation coefficient. Like the 200kHz excitation, there is a larger area of reduced cross-correlation coefficient to the left of the impact site than that observed in the out-of-plane results. This would suggest that more of the in-plane components were reflected by the presence of the impact damage than the out-of-plane components.

It is worth noting that this analysis does not indicate that the S_0 mode interacts with the damage as the whole signal length is considered. Though the A_0 is mostly out-of-plane due to Poisson's ratio, it will have a small in-plane component which may be what is causing the reduction in correlation. It is also possible that interaction with the impact damage has caused a mode conversion resulting in the A_0 mode being converted to an S_0 mode, hence the reduction of in-plane correlation. The results from this analysis however do demonstrate that it is possible to detect Lamb wave interaction with impact damage using in-plane methods of sensing.

These cross-correlation plots demonstrate the regions within the area of investigation where the waveform has been disrupted by the presence of the impact damage. This is significant for planning sensor placements to maximise the probability of damage detection. Though the higher frequency excitations showed to be more interactive with the damage, considerations for Lamb wave attenuation would also have to be considered. Thus, a trade-off between probability of detection and size of sensor network would be needed for the design of a sensor network.

Damage measurement

To quantify the damage, a section of the turbine blade surrounding the impact site was removed to enable high precision measurements of the damage to be made. On removal of the section a crack was discovered on the internal face of the blade surface which ran lengthwise along the blade as shown in Figure 16. The length of this crack exceeded the dimensions of the section removed.

Figure 16. Resulting crack on the internal face of the turbine blade.

Outer surface measurement

To measure the BVID on the external face, a Taylor-Hobson Talysurf 2 surface profilometer with a 2µm-radius stylus was used. A three-dimensional measurement was taken of a 12mm x 12mm area, with a 0.05mm y-axis spacing, a 3µm x-axis spacing and a 16nm z-axis resolution. This allowed a 3D representation of the impact site to be produced. By extracting a 2D profile across the widest part of the impact site, the BVID was found to have depth of 40µm and an average length of 7.5mm as shown in Figure 17.

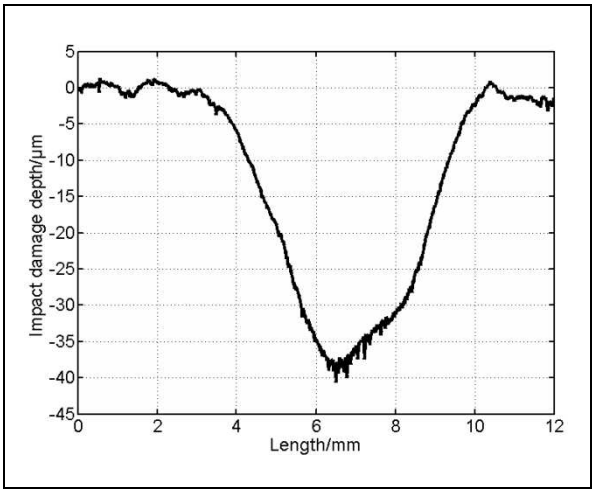

Figure 17. Surface profile of the BVID showing the length and maximum depth of the indentation created.

The depth of the impact damage on the outer face was significantly lower than that of 0.25mm which had been suggested as a quantifiable level for BVID. When inspecting the removed section it was only possible to see the damage at certain angles of viewing in well-lit conditions.

Comparing the measurement of the length of the impact site with the dimension determined from the 200kHz RMS baseline subtraction technique, there is only a 7% difference demonstrating that this Lamb wave analysis technique has potential for indicating the scale of BVID. Indeed, all three excitation frequencies identified dimensions (of the region of significant difference in waveform) which are of similar magnitude.

The 3D measurement of the impacted area is presented in Figure 18.

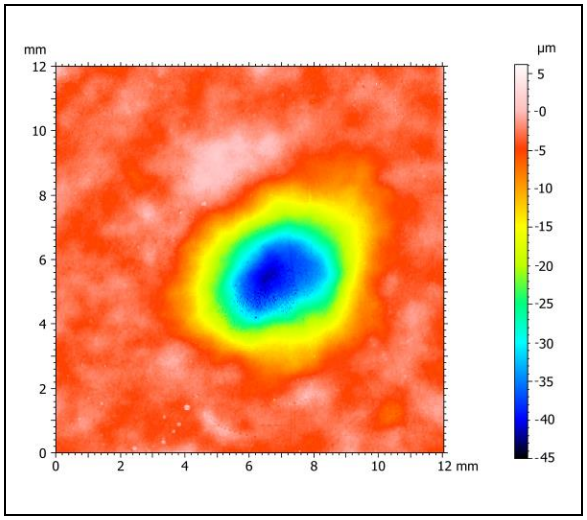

Figure 18. 3D Talysurf scan - Plan view of the BVID.

The 3D measurement shows a clear indentation caused by the impact damage. Though the maximum depth of the indent was found to be 40µm, the 3D measurement shows that only an approximately circular area of around 2mm diameter of the indentation is of this depth. This measurement however does confirm that there was no additional damage caused by the impact damage on the outer surface of the blade.

Inner surface measurement

Due to the surface profilometer being a contact measurement method it was not possible to use it to measure the inner face, which had a significantly higher level of damage rendering it unsuitable for stylus-based measurement. Precision measurements were made using a Polytec confocal-type white light interferometer.

A 15mm x 15mm area was measured with a 0.88µm x and y-axis resolution and a 50nm z-axis resolution. This allowed a 3D representation of the crack to be produced using a non-contact method.

The results from the white light interferometry are presented in Figure 19.

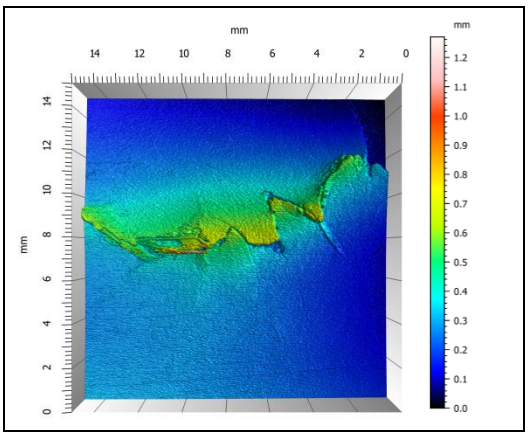

Figure 19. White light interferometry measurement of the crack on the inner face

These results show that the impact resulted in displacing material by approximately 0.9mm along the length of the crack which is photographed in Figure 16. This is significant damage which would affect the structural performance of an operational wind turbine blade.

Comparing the scale and location of the crack with the results from the 300kHz baseline subtraction it is possible that the larger area of increased RMS value was due to the presence of the crack, although this observation is by no means conclusive. As the crack ran in the same direction as the propagating wave, it would have little effect on the wave. It is possible however that shorter wavelength of the 300kHz excitation did interact with the damage.

Discussion and conclusion

This paper has demonstrated how 3D scanning laser vibrometry can be used to conduct a thorough investigation of acousto-ultrasonic induced Lamb wave interaction with impact damage on a composite turbine blade. The results from the 3D laser vibrometry clearly showed that the 100kHz excitation S_0 Lamb mode had minimal interaction with the impact damage when compared to the pre-impact results

however the higher excitation S_0 Lamb modes were more interactive due to the shorter wavelengths. The A_0 Lamb mode was found to interact at all frequencies with the impact damage, which is supported by previous studies. A high level of noise was observed particularly when the in-plane components were considered. This was justified by the inhomogeneity in the placement of the short chopped fibres and highlighted the challenge of monitoring structures reinforced with such fibres. The stand-off distance from the vibrometer to the specimen was unaltered throughout the study. Increasing the stand-off distance will inherently increase the signal to noise ratio as well as increase the laser spot size by approximately 85µm per meter of stand-off added[61]. The particular vibrometer used however is fitted with the ability to focus the laser enabling a more focused beam. If vibrometry were to be used in the field for in-service inspection, it is likely that any issues resulting by the stand-off distance can be overcome as demonstrated by previous studies[6, 62].

The dispersive phenomenon of Lamb wave modes was observed in the vibrometer results by the increased wave velocity of the higher frequency excitations.

An RMS baseline subtraction technique was applied to the out-of-plane component of the Lamb waves at the three excitation frequencies. This successfully produced a visual location and size of defect. When compared to the precise surface profilometer measurements the size of the defect was found to be within 7%. It is worth noting however that a threshold has to be set in order to reduce the effects of the low amplitude signals. This technique demonstrates potential for using scanning laser vibrometry for routine inspection of structures.

A comparison of the pre-impact and post-impact measured signals was made by calculating the cross-correlation coefficient for each measurement point, allowing a visual indication of the region where the

impact damage had influenced the Lamb wave. The out-of-plane component was first considered as it was shown to be more strongly influenced by the presence of the impact damage.

The cross-correlation coefficients for in-plane components were isolated and plotted. Noise on the in-plane components was attributed to the scattering due to the inhomogeneity of the short chopped fibre material, which was supported by the reduction of cross-correlation coefficient over the entire area of investigation.

The in-plane components of the Lamb wave were then considered with a cross-correlation coefficient being calculated for both individual in-plane components and the magnitude of both plotted. This showed an increased region of reduced correlation highlighting that it would be possible to use in-plane sensors to measure the interaction of the Lamb modes with impact damage. This would be particularly beneficial for integrated sensors.

The results from the cross-correlation analyses demonstrated that higher frequencies were more sensitive than lower frequencies to impact damage, shown by significantly larger areas of low correlation. This is in agreement with previous studies [63]. Although it would be advantageous to use higher excitation frequencies for acousto-ultrasonic SHM systems, considerations of signal attenuation have to be made as has been shown in the laser vibrometry results. Therefore, any acousto-ultrasonic sensor network design should consider the placement of sensors with respect to the attenuation of the signal and the excitation frequency with respect to the minimum defect size.

The results of the cross-correlation analysis has highlighted that in a monitored area of structure there are areas that show a minimal reduction in cross-correlation coefficient and therefore would be unlikely

to detect the damage in a acousto-ultrasonic system. Therefore, there is potential for using cross-correlation analysis on laser vibrometry to support optimisation of sensor locations.

A section of the turbine blade surrounding the impact site was removed. On removal, a crack was discovered on the internal face of the blade. Precise measurements of the damage were made on both sides of the section using surface profilometry and white light interferometry. The measured damage correlated well with the results of laser vibrometer study and the baseline subtraction RMS analysis, particularly for the 200kHz excitation where the size of the impact was found to be within 7%.

This paper has presented an in-depth study into Lamb wave interaction with impact damage in composites for SHM applications. It has been shown that even relatively low-energy impacts can result in BVID that has caused more significant damage in areas which cannot be easily inspected. It has been shown that acousto-ultrasonically induced Lamb waves have great potential for monitoring the structural integrity of wind turbine blades in-service although careful consideration must be made when considering the excitation frequency due to the complexity of the Lamb wave interaction particularly in complex composite materials.

Funding

This work was supported by the EPSRC doctoral training grant EP/K502819/1.

Acknowledgements

The authors would like to acknowledge the support of EPSRC DTG together with Airbus UK Ltd. for the funding of this project. The authors would also like to thank Dr Mark Eaton, Dr Hayley Wyatt, Dr Mathew Pearson and Mr Roger Traynor for their advice during this project and Professor Keith Worden for supplying the blade.

References

1. GWEC. Global wind statistics 2014. Brussels, Belguim: 2015.
2. Forum CWI. Summary of Wind Turbine Accident data to 31 May 2015 2015 [cited 2015 17th July]. Available from: http://www.caithnesswindfarms.co.uk/AccidentStatistics.htm.
3. Khan M, Iqbal M, Khan F, editors. Reliability analysis of a horizontal axis wind turbine. IEEE 14th NECEC conference (Newfoundland, Canada); 2004.
4. Larsen FM, Sorensen T, editors. New lightning qualification test procedure for large wind turbine blades. Proceedings of International Conference on Lightning and Static Electricity, Blackpool, UK; 2003.
5. Pinar Pérez JM, García Márquez FP, Tobias A, Papaelias M. Wind turbine reliability analysis. Renewable and Sustainable Energy Reviews. 2013;23:463-72.
6. Lee J-R, Shin H-J, Chia CC, Dhital D, Yoon D-J, Huh Y-H. Long distance laser ultrasonic propagation imaging system for damage visualization. Optics and Lasers in Engineering. 2011;49(12):1361-71.
7. Marsh G. The challenge of wind turbine blade repair Renewable Energy Focus2011 [cited 2015 17th July]. Available from: http://www.renewableenergyfocus.com/view/21860/the-challenge-of-wind-turbine-blade-repair/.
8. Kusiak A, Li W. The prediction and diagnosis of wind turbine faults. Renewable Energy. 2011;36(1):16-23.
9. Sørensen BF, Jørgensen E, Debel CP, Jensen FM, Jensen HM, Jacobsen TK, et al. Improved design of large wind turbine blade of fibre composites based on studies of scale effects (Phase 1). Summary report2004.
10. Speckmann H, Roesner H. Structural Health Monitoring: A Contribution to the Intelligent Aircraft Structure. ECNDT 2006; Berlin2006.
11. McGowan DM, Ambur DR. Damage-Tolerance Characteristics of Composite Fuselage Sandwich Structures With Thick Facesheets. 1997.
12. Services TW. Wind Turbine Blade Services 2015 [cited 2015 17th July]. Available from: http://www.technicalwindservices.com/wind-turbine-blade-repair.php.
13. Chia Chen C, Jung-Ryul L, Hyung-Joon B. Structural health monitoring for a wind turbine system: a review of damage detection methods. Measurement Science and Technology. 2008;19(12):122001.
14. Worden K, Dulieu-Barton JM. An Overview of Intelligent Fault Detection in Systems and Structures. Structural Health Monitoring. 2004;3(1):85-98.
15. Han B-H, Yoon D-J, Huh Y-H, Lee Y-S. Damage assessment of wind turbine blade under static loading test using acoustic emission. Journal of Intelligent Material Systems and Structures. 2014;25(5):621-30.
16. Tang J, Rafael S, Soua S, Mares C, Gan T-H. Structural Health Monitoring Methodology for Wind Turbine Blades using Acoustic Emission. National Seminar & Exhibition on Non-

Destructive Evaluation; December 4th-6th; Pune, India: The e-Journal of Non-Destrcutive Testing; 2015.
17. Blanch M, Dutton A, editors. Acoustic emission monitoring of field tests of an operating wind turbine. Key Engineering Materials; 2003: Trans Tech Publ.
18. Park G, Farinholt KM, Taylor SG, Farrar CR. A full-scale fatigue test of 9-m CX-100 wind turbine blades. DTIC Document, 2011.
19. Baxter MG, Pullin R, Holford KM, Evans SL. Delta T source location for acoustic emission. Mechanical Systems and Signal Processing. 2007;21(3):1512-20.
20. Melnyk S, Tuluzov I, Melnyk A, editors. Method of remote dynamic thermographic testing of wind turbine blades. The 12th International Conference on Quantitative InfraRed Thermography, Bordeaux; 2014.
21. Stanley P. Applications and potential of thermoelastic stress analysis. Journal of materials processing technology. 1997;64(1):359-70.
22. Krstulovic-Opara L, Klarin B, Neves P, Domazet Z. Thermal imaging and Thermoelastic Stress Analysis of impact damage of composite materials. Engineering Failure Analysis. 2011;18(2):713-9.
23. Hahn F, Kensche C, Paynter R, Dutton A, Kildegaard C, Kosgaard J. Design, fatigue test and NDE of a sectional wind turbine rotor blade. Journal of Thermoplastic Composite Materials. 2002;15(3):267-77.
24. Farrar CR, Doebling SW, editors. An overview of modal-based damage identification methods. Proceedings of DAMAS Conference; 1997: Citeseer.
25. Gross E, Simmermacher T, Rumsey M, Zadoks RI, editors. Application of damage detection techniques using wind turbine modal data. American Society of Mechanical Engineers Wind Energy Symp(Reno, NV, USA); 1999.
26. Dervilis N, Choi M, Antoniadou I, Farinholt KM, Taylor SG, Barthorpe RJ, et al. Novelty detection applied to vibration data from a CX-100 wind turbine blade under fatigue loading. Journal of Physics: Conference Series. 2012;382(1).
27. Siringoringo DM, Fujino Y. Experimental study of laser Doppler vibrometer and ambient vibration for vibration-based damage detection. Engineering Structures. 2006;28(13):1803-15.
28. Eaton M, May M, Featherston C, Holford K, Hallet S, Pullin R. Characterisation of Damage in Composite Structures using Acoustic Emission. Journal of Physics: Conference Series. 2011;305(1):012086.
29. Williamson C, Fixter L. State of the Art Review—Structural Health Monitoring. QinetiQ, QinetiQ/S&DU/T&P/E&M/TR0601122. 2006.
30. Lee J-R, Tsuda H. A novel fiber Bragg grating acoustic emission sensor head for mechanical tests. Scripta materialia. 2005;53(10):1181-6.
31. Perez IM, Cui H, Udd E, editors. Acoustic emission detection using fiber Bragg gratings. SPIE's 8th Annual International Symposium on Smart Structures and Materials; 2001: International Society for Optics and Photonics.

32. Takeda N, Okabe Y, Kuwahara J, Kojima S, Ogisu T. Development of smart composite structures with small-diameter fiber Bragg grating sensors for damage detection: Quantitative evaluation of delamination length in CFRP laminates using Lamb wave sensing. Composites Science and Technology. 2005;65(15):2575-87.
33. Speckmann H, Henrich R, editors. STRUCTURAL HEALTH MONITORING (SHM) - OVERVIEW ON AIRBUS ACTIVITIES. 16th WCNDT 2004 - World Conference on NDT; 2004 August 30th - September 3rd; Montreal, Canada.
34. Yang R, He Y, Zhang H. Progress and trends in nondestructive testing and evaluation for wind turbine composite blade. Renewable and Sustainable Energy Reviews. 2016;60:1225-50.
35. Lamb H. On waves in an elastic plate. Proceedings of the Royal Society of London Series A, Containing papers of a mathematical and physical character. 1917:114-28.
36. Rose JL. Ultrasonic Waves in Solid Media. Cambridge: Cambridge University Press; 1999.
37. Worden K. Rayleigh and Lamb waves - Basic principles. Strain. 2001;37(4):167-72.
38. Eaton MJ. Acoustic Emission (AE) monitoring of buckling and failure in carbon fibre composite structures. Cardiff: Cardiff University; 2007.
39. Pullin R, Eaton MJ, Pearson MR, Featherston C, Lees J, Naylon J, et al. On the Development of a Damage Detection System using Macro-fibre Composite Sensors. Journal of Physics: Conference Series. 2012;382(1):012049.
40. Polytec. Introduction to 3-D Scanning Vibrometry by Polytec GmbH, Polytec Inc. Wahlbronn, Germany2009. p. 3.21.
41. Polytec. Polytec Scanning Vibrometer Theory Manual. Wahlbronn, Germany: Polytec Gmbh.
42. Castellini P, Martarelli M, Tomasini EP. Laser Doppler Vibrometry: Development of advanced solutions answering to technology's needs. Mechanical Systems and Signal Processing. 2006;20(6):1265-85.
43. Nishizawa O, Satoh T, Lei X. Detection of shear wave in ultrasonic range by using a laser Doppler vibrometer. Review of scientific instruments. 1998;69(6):2572-3.
44. He L, Kobayashi S. Determination of Stress-Acoustic Coefficients of Rayleigh Wave by Use of Laser Doppler Velocimetry. JSME International Journal Series A Solid Mechanics and Material Engineering. 2001;44(1):17-22.
45. Kehlenbach M, Kohler B, Cao X, Hanselka H, editors. Numerical and experimental investigation of Lamb wave interaction with discontinuities. Proceedings of the 4th international workshop on structural health monitoring; 2003.
46. Staszewski WJ, Lee BC, Mallet L, Scarpa F. Structural health monitoring using scanning laser vibrometry: I. Lamb wave sensing. Smart Materials and Structures. 2004;13(2):251-60.
47. Maslov K, Kinra VK. Scanning laser vibrometry for Lamb wave evaluation of composite tubulars. Nondestructive Testing and Evaluation. 2000;15(6):395-409.
48. Mizutani Y, Yamada H, Nishino H, Takemoto M, Ono K, editors. Noncontact detection of delamination in impacted cross-ply CFRP using laser-generated Lamb waves. 6th Annual

International Symposium on NDE for Health Monitoring and Diagnostics; 2001: International Society for Optics and Photonics.
49. Hailu B, Hayward G, Gachagan A, McNab A, Farlow R, editors. Comparison of different piezoelectric materials for the design of embedded transducers for structural health monitoring applications. Proceedings of the IEEE Ultrasonics Symposium; 2000.
50. Yang S, Allen MS. Output-only Modal Analysis using Continuous-Scan Laser Doppler Vibrometry and application to a 20kW wind turbine. Mechanical Systems and Signal Processing. 2012;31:228-45.
51. Ghoshal A, Sundaresan MJ, Schulz MJ, Frank Pai P. Structural health monitoring techniques for wind turbine blades. Journal of Wind Engineering and Industrial Aerodynamics. 2000;85(3):309-24.
52. Rumsey M, Hurtado J, Hansche B, Simmermacher T, Carne T, Gross E. IN-FIELD USE OF LASER DOPPLER VIBROMETER ON A WIND TURBINE BLADE. 1997.
53. Grigg S, Pearson M, Marks R, Featherston C, Pullin R. Assessment of Damage Detection in Composite Structures Using 3D Vibrometry. Journal of Physics: Conference Series. 2015;628(1):012101.
54. Schubert L, Lieske U, Köhler B, Frankenstein B. INTERACTION OF LAMB WAVES WITH IMPACT DAMAGED CFRP'S STUDIED BY LASER-VIBROMETRY AND ACOUSTO ULTRASONIC.
55. Sohn H, Dutta D, Yang JY, Desimio M, Olson S, Swenson E. Automated detection of delamination and disbond from wavefield images obtained using a scanning laser vibrometer. Smart Materials and Structures. 2011;20(4).
56. Staszewski WJ, Lee BC, Traynor R. Fatigue crack detection in metallic structures with Lamb waves and 3D laser vibrometry. Measurement Science and Technology. 2007;18(3):727.
57. Marks R, Clarke A, Featherston C, Kawashita L, Paget C, Pullin R. Using genetic algorithms to optimize an active sensor network on a stiffened aerospace panel with 3D scanning laser vibrometry data. Journal of Physics: Conference Series. 2015;628(1):012116.
58. Marks R, Clarke A, Featherston C, Paget C, Pullin R. Sensor location studies for damage detection in Aerospace Structures using 3D scanning Laser Vibrometry. In: Siljander A, editor. ICAF 2015; Helsinki, Finland: International Committee of Aeronautical Fatigue; 2015. p. 808-18.
59. Pan Y, Iorga L, Pelegri AA. Analysis of 3D random chopped fiber reinforced composites using FEM and random sequential adsorption. Computational Materials Science. 2008;43(3):450-61.
60. Rokhlin S, Kim J-Y, Xie B, Zoofan B. Nondestructive sizing and localization of internal microcracks in fatigue samples. NDT & E International. 2007;40(6):462-70.
61. Polytec Ltd. Polytec Scanning Vibrometer PSV-500-3D Hardware Manual 2012.
62. Chen S-E, Petro S. Nondestructive bridge cable tension assessment using laser vibrometry. Experimental Techniques. 2005;29(2):29-32.
63. ULTRASONIC TESTING OF AEROSPACE MATERIALS, (1998).